OXFORD

Journal of Petrology, 2024, **65**, egae086
https://doi.org/10.1093/petrology/egae086
ADVANCE ACCESS PUBLICATION DATE 3 AUGUST 2024
Original Manuscript

Metamorphic origin of large nuggets of platinum-group metals: evidence from multiphase inclusions in Os-Ir-Ru alloys from the Adamsfield placer, Tasmania

ANTON KUTYREV [1,*], VADIM S. KAMENETSKY [2,3], IVAN F. CHAYKA [4], NIKOLAI A. NEKRYLOV [5], LYUDMILA KRYUCHKOVA [6], VLADIMIR V. SHILOVSKIKH [7], ALKIVIADIS KONTONIKAS-CHAROS [8], STEPAN P. KRASHENINNIKOV [9], ANNA SAPEGINA [4,10,11] and ALEXEI L. PERCHUK [4,10,11]

[1]School of Earth and Environmental Sciences, Cardiff University, Main Building, Park Place, Cardiff, Wales CF10 3AT, UK
[2]Center of Deep Sea Research, Institute of Oceanology, Chinese Academy of Sciences, 7 Nanhai Road, Qingdao 266071, P. R. China
[3]Laboratory of Mineralogy, Institute of Volcanology and Seismology FEB RAS, Piipa 9, Petropavlovsk-Kamchatsky 683006, Russia
[4]Laboratory of Physiochemical Problems of Magmatism, Korzhinskii Institute of Experimental Mineralogy RAS, 4, Academician Ossipyan str., Chernogolovka 142432, Russia
[5]Laboratory of Volcanology, Institute of Geological Sciences NAS RA, Marshal Baghramyan Avenue 24, Yerevan, Armenia
[6]The Center for X-Ray Diffraction Studies, Research Park, St. Petersburg State University, Decabristov lane 16, Saint-Petersburg 199155, Russia
[7]Geomodel Center, Saint-Petersburg State University, Ulyanovskaya str., 1, 198504 Saint-Petersburg, Russian Federation
[8]School of Earth and Atmospheric Sciences, Queensland University of Technology, P Block, Level 6, Gardens Point Road Brisbane 4001, QLD, Australia
[9]Laboratory of Geochemistry of Igneous and Metamorphic Rocks, Vernadsky Institute of Geochemistry and Analytical Chemistry RAS, 19 Kosygina str., Moscow 119991, Russia
[10]Department of Petrology and Volcanology, Faculty of Geology, Moscow State University, Leninskie Gori, 1, Moscow 119991, Russia
[11]Laboratory of the Lithosphere Metamorphism, Magmatism and Geodynamics, Korzhinskii Institute of Experimental Mineralogy RAS, 4, Academician Ossipyan str., Chernogolovka 142432, Russia

*Corresponding author: Email: KutyrevA@cardiff.ac.uk

Platinum-group elements (PGE) are most effectively concentrated via sulfide-silicate melt immiscibility; however, under sulfide-undersaturated conditions, PGE may exhibit highly siderophile behavior and occur as native metals and alloys. In this case, they can form micrometer-size inclusions within Cr-spinel, but also large nuggets (up to several kilograms), found in chromitites and related placer deposits. The exact formation mechanism of such large nuggets and accumulations of PGE unrelated to sulfide melts remains controversial due to mass balance issues. In this study of multiphase inclusions in Os-Ir-Ru nuggets from the Adamsfield placer district (Tasmania, Australia), we constrain their crystallization environment. Multiphase inclusions comprise variable proportions of hornblende, enstatite, quartz, anthophyllite, anorthite, chlorite and native iridium and coexist with single-phase olivine and Cr-spinel inclusions. The heterogeneity in phase and chemical composition of the inclusions indicates a complex origin from an inhomogeneous source media. This is corroborated by grain scale disequilibrium mineral assemblages, where forsterite and quartz are both included within a single osmium grain. Our proposed multi-stage origin of Adamsfield Os-Ir-Ru nuggets involved magmatic olivine-Cr-spinel-Os-Ir-Ru cumulates in peridotite bodies that were subsequently overprinted by various hydrothermal and metamorphic processes, including serpentinization or growth of Os-Ir-Ru from supercritical fluids. The final metamorphic stage resulted in the obliteration of Os-Ir-Ru zonation, culminating in the current assemblage of inclusions.

Key words: ophiolite; osmium; chromitite; melt inclusions; platinum-group elements

INTRODUCTION

Platinum-group elements (PGE) are among the rarest and most irregularly distributed metals in the Earth's crust and mantle, with concentrations rarely exceeding parts per billion (ppb) in common rocks. The most effective mechanism of PGE transfer and accumulation is via sulfide-silicate melt immiscibility (Naldrett, 2004; Mansur *et al.*, 2020). However, in sulfide-undersaturated environments, such as oxidized arc magmas, PGE show highly siderophile behavior and can occur as micrometer-size inclusions of Pt-Fe and Os-Ir-Ru alloys hosted within liquidus Cr-spinel (Kamenetsky *et al.*, 2015) or other oxides (Anenburg & Mavrogenes, 2016). Chromitites in Ural-Alaskan-type peridotite complexes are particularly notable for their sizeable (up to several kilograms) Pt-Fe alloy nuggets (Orlov, 2019; Kutyrev *et al.*, 2020), whereas chromitites in ophiolitic peridotites and related placers may contain Os-Ir-Ru nuggets up to 70 g in weight (Reid, 1921).

Most modern genetic models of PGE alloy formation suggest direct crystallization from a melt on the surface of liquidus Cr-spinel, as observed in experiments (Finnigan *et al.*, 2008) and volcanic rocks (Kamenetsky *et al.*, 2015). In regards to plutonic rocks, three main groups of hypotheses have been proposed to explain the formation of platinum-group minerals (PGM) in the presence of chromite and effectively no sulfides. The first involves direct crystallization of the PGM from a primitive melt (Barnes

RECEIVED FEBRUARY 5, 2024; **REVISED** JULY 27, 2024; **ACCEPTED** JULY 29, 2024

et al., 1985; Prichard et al., 2017) with their subsequent incorporation into chromite (Tredoux et al., 1995) and formation of early-magmatic PGE-Fe alloys attached to chromite grains (Hiemstra, 1979). The second suggests exsolution of the PGE (mainly IPGE), which were initially incorporated into the chromite lattice at high temperatures, eventually forming their own distinct phases (Oshin & Crocket, 1982; Barnes et al., 1985; Prichard et al., 2017). Finally, it has been also supposed that such PGM mineralization may actually result from total desulfidation of a pristine PGM-sulfide assemblage (Naldrett & von Gruenewaldt, 1989).

Although such models explain the occurrence of micrometer-size PGM, they cannot account for the origin of larger nuggets, because the latter require a huge excess of PGE in a small volume. Origins of millimeter- to centimeter-size nuggets have been attributed to: (1) direct crystallization of the PGM from silicate melt in flow-through cavities (Augé et al., 2005) or mechanical accumulation of these PGM in a magma chamber (Peck et al., 1992; Borg & Hattori, 1997); (2) crystallization at late-magmatic stages from differentiated liquids (Tolstykh et al., 2015); (3) hydrothermal, metasomatic or metamorphic concentration of the PGM from disseminated primary-magmatic grains into large nuggets (Pushkarev et al., 2007) and; (4) silicate-oxide immiscibility with the PGE incorporation into the oxide melt and its subsequent differentiation from magmatic to hydrothermal stage (Okrugin, 2011; Stepanov et al., 2020). All these hypotheses encounter a mass-balance problem and imply either a long-term precipitation of PGE from a transporting medium in a restricted volume or their multistage concentration, supposing that various stages (from magmatic to metamorphic and low-*T* hydrothermal) play their unique roles. The similar mass-balance problem extends to the genesis of massive chromitites (both podiform and stratiform), which is explained by a variety of models including, but not limited to, gravitational settling, crystal mush slurries, melt-rock interaction, chromite-only saturation and subsolidus processes (Arai, 1997; Maier et al., 2013; Arai & Akizawa, 2014; Latypov et al., 2020; Smith & Maier, 2021).

This study aims to unravel the formation media of millimeter-size Os-Ir-Ru nuggets from the Adamsfield placer (western Tasmania, Australia) by investigating Os-hosted primary multiphase inclusions. Our results suggest that substantial PGE accumulation in millimeter-size and larger grains requires a multi-stage process, embracing both magmatic and metamorphic environments.

GEOLOGICAL SETTING AND SAMPLES

Relicts of the western Tasmanian ophiolite are represented by mafic–ultramafic complexes, generally less than 50 km^2 in size (Fig. 1), that exhibit a tectonic emplacement atop Neoproterozoic rift sequences or allochthonous mélanges during the Middle Cambrian (Crawford & Berry, 1992; Mulder et al., 2016). Volcanic constituents of these complexes include low-titanium tholeiitic basalts and boninites (Crawford & Berry, 1992). These mafic–ultramafic complexes, classified as parts of back-arc ophiolites (Mulder et al., 2016), display metamorphic assemblages formed at granulite–upper amphibolite conditions (up to 875°C, 0.8 GPa) and record a cooling and decompression path through relatively low-*P* amphibolite facies (up to 600°C, 0.6 GPa, Mulder et al., 2016).

The Adamsfield complex comprises poorly layered peridotite bodies of partly serpentinized dunite, olivine orthopyroxenites and orthopyroxenites, all containing disseminated Cr-spinel and chromitite schlieren (Peck & Keays, 1990; Calver et al., 2014). The spatially associated Adamsfield River Os-Ir-Ru placer was allegedly sourced from the Adamsfield ophiolite, where Os-Ir-Ru lodes have been reported in serpentinitic conglomerates (Mertie Jr., 1969; Ford, 1981; Peck et al., 1992).

METHODS

Electron microprobe analysis

Electron probe wavelength dispersion microanalysis (WDS EPMA) has been carried out on the JEOL JXA-8320 electron probe microanalyzer at the Analytical Center of Institute of Geology and Mineralogy, Siberian branch, of the Russian Academy of Sciences (IGM SB RAS), Novosibirsk, Russia. Analyses of silicate minerals were acquired at a 40 nA beam current and 20 kV acceleration voltage. The concentration of all elements was measured using the intensity of their Kα lines with an acquisition time of 10 s and background signal measurement of 5 s. Standards used were: albite (Na_2O and Al_2O_3), diopside (SiO_2, CaO and MgO), synthetic glass Gl-6 (TiO_2), Cr-bearing garnet (Cr_2O_3), orthoclase (K_2O), pyrope (FeO) and Mn-bearing garnet (MnO). Analyses of glasses were acquired at 30 nA beam current and 20 kV acceleration voltage using a de-focused beam (~5-μm diameter) to avoid diffusion of alkalis and volatile elements (Morgan & London, 1996). As well as for silicate minerals, all elements were measured using the intensity of their Kα lines with an acquisition time of 10 s and background signal measurement of 5 s. Suppl. Table S1 comprises the data on standard errors and detection limits.

Analyses of Os-Ir-Ru alloys was conducted on Tescan Vega-3 electron microscope equipped with Oxford-50 EDS. The following standards were used: pure metals for PGE (Pt, Os, Ir, Ru, Rh, Pd) and Ni; FeS_2 for Fe and S, $CuFeS_2$ for Cu. The analytical conditions were: 15 kV accelerating voltage, 20 s counting live time, 0.7 nA current intensity. The following X-ray lines were used: Ma for Pt, Os, Ir, Au and Hg; La for Ru, Rh, Pd, Ag and As; and Ka for Fe, Cu, S and Ni.

Raman spectroscopy

Raman spectroscopy (LabRam HR800 Horiba Jobin Yvon spectrometer, equipped with an optical microscope Olympus BX41, IGM SB RAS) was performed on the inclusions' phases to confirm identification of anthophyllite (Suppl. Fig. S1). The 514.5-nm Ar^+ laser line was used for spectral excitation. The RRUFF database and data from Wang et al. (1988) and (Apopei & Buzgar, 2010) were used to identify the solid phases.

Heating experiments

Homogenization through heating and quenching of the osmium-hosted multiphase inclusions was performed to estimate the bulk compositions of the inclusions. These experiments were conducted in tube furnaces, which allowed for gradual heating of the mineral separates with subsequent rapid quenching by dropping the container into water. For the 1300°C experiment a Nabertherm RHTV 120–300/17 vertical tube furnace (Vernadsky Institute of Geochemistry, Moscow, Russia) was employed (Krasheninnikov et al., 2017). We performed the experiment at 1 bar CO_2–H_2 atmosphere at oxygen fugacity corresponding to quartz-magnetite-fayalite (QFM) buffer in an open quartz crucible and terminated it by quenching in water. Because the majority of the inclusions quenched at 1300°C contained daughter phases with only few inclusions reaching complete homogenization, the experiment was repeated at 1400°C. For the 1400°C run we used a custom-designed vertical tube furnace (Chayka et al., 2023) that consisted of a sapphire tube, wired by a heater (ferro-aluminum high-resistance alloy), isolated by chamotte clay. The tube was

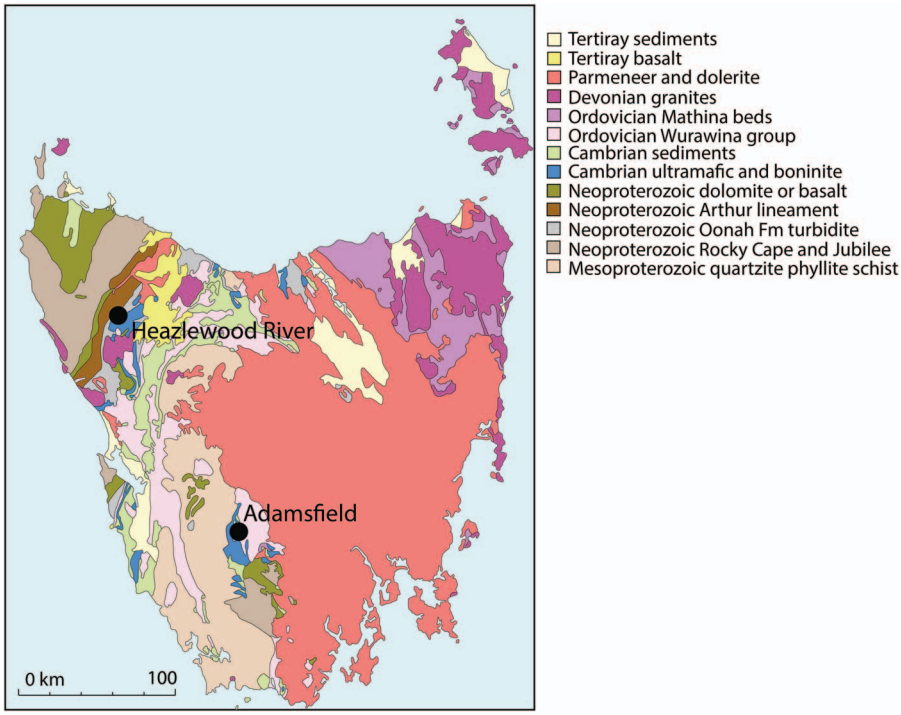

Fig. 1. Geological sketch of Tasmania and position of Adamsfield and Heazlewood River ultramafic complexes. After (Seymour, 2007).

placed into a furnace casing that was filled with Al_2O_3 filler for insulation. The temperature control system included a DC-regulated power supply, an automatic temperature controller and a Pt-Pt/Rh thermocouple that was placed into the sapphire tube. To prevent oxidation, osmium grains were placed into a Pt capsule, filled with an excess of reducing filler (diamond powder). The capsule with the grains was gradually (~10°C/s) heated up to 1300°C and exposed to this temperature for 5 min before being rapidly quenched in water. The estimated cooling time for the inclusions was 3–4 s. After the experiment, the grains were mounted in epoxy, ground until the exposure of the inclusions and polished using a water-free lubricant (WD-40 oil). To ensure absence of daughter phases within inclusions, they were additionally inspected using a binocular loupe.

Phase equilibria modeling

The PERPLE_X software (version 7.1.6, updated on 21 January 2024) (Connolly, 2005), including database files '*hp634ver.dat*' (Holland & Powell, 2011) with a thermodynamic dataset and '*solution_model.dat*' for solid-solution models, was used to construct P–T phase diagrams for the effective composition of a representative multiphase inclusion. As some phases may have remained unexposed in polished sections, in addition to the host inclusion, we also estimated a composition of a model 'ideal' inclusion. A model inclusion was calculated by combining the compositions of five primary minerals (hornblende, orthopyroxene, anthophyllite, quartz and anorthite) in proportions roughly similar to those observed across all inclusions until the composition matched that of the homogenized glasses. The resulting inclusion consists of enstatite (21 vol %), hornblende (48 vol %), anthophyllite (12 vol %), quartz (10 vol %) and anorthite (9 vol %). The modeling was carried out using solid solution models 'feldspar' for plagioclase (Fuhrman & Lindsley, 1988), cAmph(G) for amphibole (Green *et al.*, 2016), Gt(TH) for garnet, Cpx(TH) for clinopyroxene and Opx(TH) for orthopyroxene (Tomlinson & Holland, 2021). The effective bulk chemical composition of the multiphase inclusion was quantified using the modes of the minerals (based on the number of pixels in the BSE image) and the density and composition of each mineral.

RESULTS

Mineral assemblages of Adamsfield placer

The alluvial heavy-metal nuggets are mostly comprised of Os-Ir-Ru (Fig. 2) with a substantial admixture of Ir and Ru (Suppl. Table S2, 46–55 wt % Os, 39–43 wt % Ir and 5–11 wt % Ru, Fig. 3). This mineral was previously called 'osmiridium' (Cabri & Harris, 1975; Peck *et al.*, 1992), a name discredited by the International Mineralogical Association (Harris & Cabri, 1991). To avoid confusion, the term 'Os-Ir-Ru' alloy will be used here for minerals predominantly composed of Os. Other PGM in the placer are native iridium, native ruthenium, isoferroplatinum Pt_3Fe, laurite $(Ru,Os)S_2$, Rh-Ir sulfarsenides. The studied grains are single crystals or intergrowths, up to 2–3 mm in size, with well-preserved primary features, such as crystal faces and intergrowths (Fig. 2c) with Cr-spinel (Fig. 2d). The grains are monocrystalline, with minor misorientations (i.e. deviation in orientation of certain crystal parts and blocks Fig. 4).

Multiphase inclusions in Os-Ir-Ru Alloys

Most grains of Os-Ru-Ir alloy contain a variety of inclusions (10–50 μm in size) that are found exposed naturally on cleaved surfaces (Fig. 2b), artificially by sequential grinding (Fig. 5, 6) or detected by the high-resolution X-ray computed tomography (Fig. 7). The inclusions are typically multiphase (Fig. 5d–h); however, rare single phases exist such as high-Mg olivine (Mg# = 0.90–0.94; Table S2; Fig. 6) and Cr-spinel (Cr# = 81, Peck *et al.*, 1992). Hexagonal multiphase inclusions within single grains of Os-Ir-Ru alloy are well aligned with each other and follow crystallographic orientations of their host mineral (Fig. 5b). Many hexagonal inclusions consist of only one clearly distinguishable

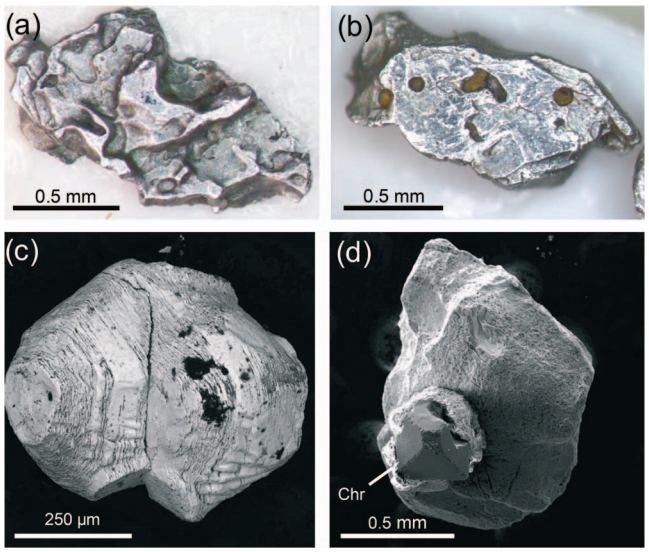

Fig. 2. Photo (a, b), backscatter (c) and secondary electron (d) images of the Os-Ir-Ru nuggets from Adamsfield. Figure (b) demonstrates exposed multiphase inclusions; (d) shows intergrowth between the Os-Ir-Ru alloy and Cr-spinel.

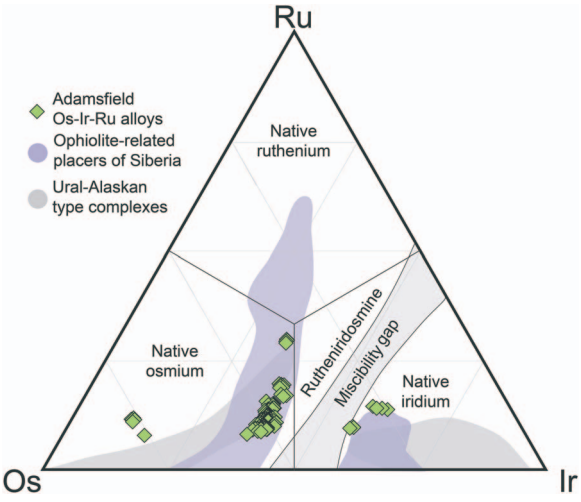

Fig. 3. Compositions of Os-Ir-Ru alloys in Adamsfield placer district. Ophiolite field after Tolstykh *et al.* (2004); Ural-Alaskan-type field after Tolstykh *et al.* (2004), Kutyrev *et al.* (2018), Kutyrev *et al.* (2021b).

mineral (usually hornblende), making them, strictly speaking, monophase inclusions. However, due to similarities in shape and composition, such monomineralic inclusions are counted together with multiphase inclusions.

Most of the studied multiphase inclusions ($n = 74$, Fig. 8) comprise the following minerals: hornblende ($n = 47$, Fig. 5a, c–i), enstatite ($n = 19$; Fig. 5a, c, e), quartz ($n = 17$; Fig. 5a, c, f, h), anthophyllite ($n = 16$; Fig. 5a, e), anorthite ($n = 5$; Fig. 5d, f), olivine ($n = 1$; Fig. 5g), spinel ($n = 1$) and Cr-spinel ($n = 1$, Fig. 5g). The most common mineral assemblage is represented by hornblende and quartz and may include other phases. Few inclusions comprise hydrous phyllosilicates (Fig. 5e, g), dominated by chlorite ($n = 10$), serpentine ($n = 4$) and rarely talc ($n = 1$). In addition to silicates, a few multiphase inclusions contain native iridium ($n = 4$, Fig. 5h, i). Among the most abundant minerals, enstatite exhibits euhedral morphology (Fig. 5c, e); hornblende and anthophyllite are subhedral relative to enstatite (Fig. 5e) but euhedral to quartz,

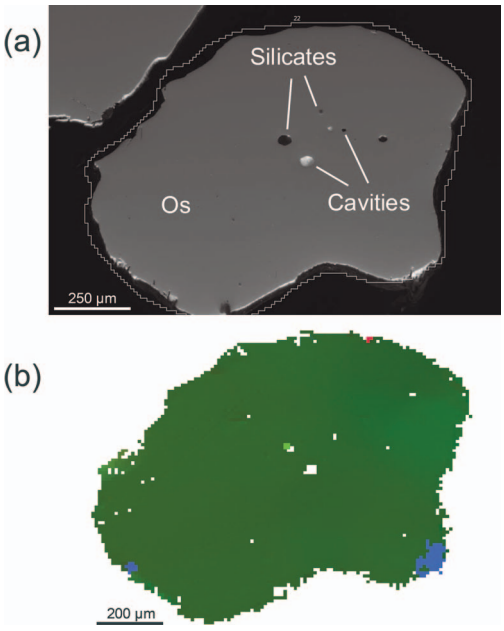

Fig. 4. The results of electron-backscatter diffraction (EBSD). (a) – backscatter electron image, (b) – Euler image and (c) – pole figures showing the orientation of the Os-Ir-Ru. Additional EBSD images are in the Supplementary Data Fig. S3, S4).

which is usually subhedral (Fig. 5c, h). Composition of the silicates is variable, with orthopyroxene Mg# = 0.90–0.96 and hornblende FeO_{tot} and Al_2O_3 varying from 1.0 to 8.4 and 6.9 to 15.9 wt %, respectively (Supplementary Table S3).

Composition of homogenized inclusions

A test for the magmatic origin of the studied inclusions in Os-Ir-Ru alloy and their average composition was performed by heating/quenching experiments. Heating to 1300°C, which is a realistic liquidus temperature for mafic silicate melts, resulted in the formation of numerous forsterite and enstatite crystals embedded in a silicate glass. Heating to higher temperatures (1400°C) reduced the number of peritectic or residual crystalline phases and increased the amount of silicate glass, yet still failed to produce homogeneous glasses only. The compositions of crystal-free, at least at the exposed inclusions' surfaces, glasses (Fig. 9 and Table 1) exhibit high variability with respect to all major elements (i.e. 15–28 wt % MgO, 5–10 wt % CaO, etc.). FeO is positively correlated with MgO (Fig. 9b), whereas CaO and Al_2O_3 demonstrate negative correlations with MgO (Fig. 9c, d) and a positive correlation with each other (Fig. 9e).

Phase equilibria modeling

The representative multiphase inclusion consists of orthopyroxene, Ca-amphibole and quartz (Fig. 5c). Phase equilibrium modeling for its effective chemical composition shows that Ca-amphibole-orthopyroxene-quartz (Amph-Opx-Qz) mineral paragenesis is missing from the graph in the P–T range of 600–1100°C and 0.1–3.0 GPa appropriate to the mantle wedge (Suppl. Fig. S2). This suggests that these minerals are unlikely to be in equilibrium in the inclusion. In fact, such mineral paragenesis in high-grade metamorphic rocks is not well known.

Thus, caution is necessary in the application of the phase equilibria modeling method to the tiny inclusions because there may exist non-equilibrated minerals and/or irrelevant modes of minerals trapped by the host mineral.

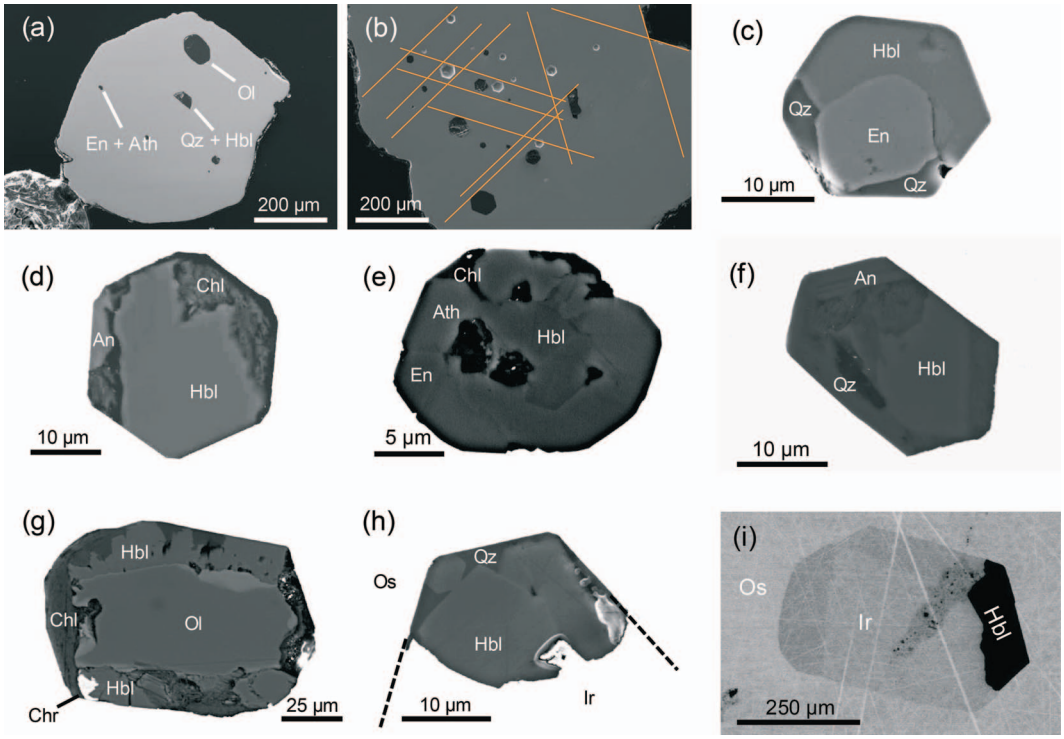

Fig. 5. Electron images of multiphase inclusions in Os-Ir-Ru alloy nuggets from the Adamsfield placer. (a) Olivine inclusion and multiphase inclusions coexisting within a single grain. (b) Numerous multiphase inclusions aligned along the crystallographic orientation of the host Os-Ir-Ru grain. (c-f) Detailed images of multiphase inclusions. (g) Multiphase inclusions with olivine, chromite and hydrous silicates. (h, i) Multiphase inclusions composed of hornblende, quartz and native iridium. Mineral abbreviations: An – anorthite, Ath – anthophyllite, Chl – chlorite, Chr – chromite, En – enstatite, Hbl – hornblende, Ol – olivine, Qz – quartz, Os – Os-Ir-Ru, Ir – native iridium.

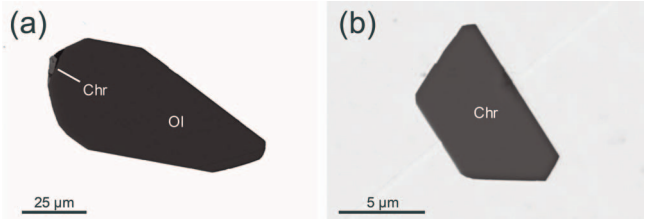

Fig. 6. Electron images of olivine and Cr-spinel inclusions in Os-Ir-Ru alloy nuggets from the Adamsfield placer.

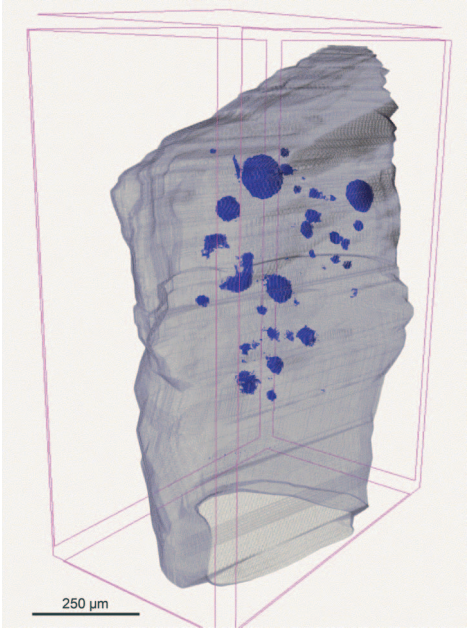

Fig. 7. High-resolution X-ray computed tomography of an Os-Ir-Ru alloy grain showing distribution of multiphase inclusions. The animated image is available in the Supplementary Data Media.

Within these limitations, we tested a phase diagram for the chemical composition of the statistically 'average' inclusion. The P–T field of the plagioclase-orthopyroxene-Ca-amphibole-cummingtonite-quartz (Pl-Opx-Amp-Cumm-Qz) mineral assemblage is restricted by a maximum pressure and temperature of ~0.7 GPa and ~790°C, respectively (Fig. 10), which broadly corresponds to the amphibolite facies conditions. However, assuming that inclusions comprise anthophyllite, both temperature and pressure shift to lower values. Further specification of the P–T conditions on the basis of hypothetical inclusion seems excessive.

DISCUSSION

Primary origin of Os-hosted inclusions

A critical question for genetic constraints on inclusion-bearing minerals is the time and environment of entrapment of inclusions. Inclusions of primary origin, i.e. captured during the mineral growth and representing either a parental melt, or fluid, or crystals (e.g. 'crystal mush'), can be used as a natural experimental laboratory to model the crystallization medium. The studied single-phase and multiphase inclusions are distributed following the main crystallographic directions of the host Os (e.g. Fig. 5b) but show no alignment with potential linear fractures (Fig. 5b, 7), providing an argument for their primary origin. Moreover, despite variable phase

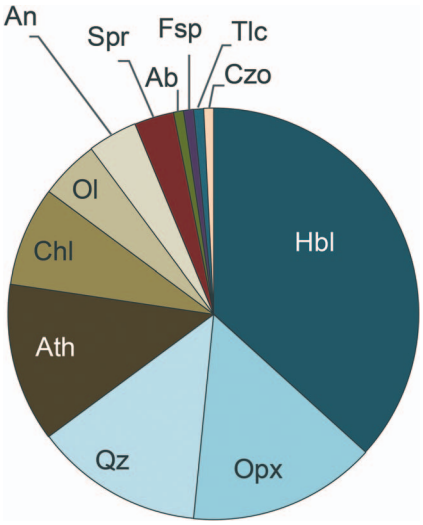

Fig. 8. Relative abundance of minerals in the inclusions before the heating. Mineral abbreviations: Ab – albite, An – anorthite, Ath – anthophyllite, Chl – chlorite, Chr – chromite, Czo – clinozoisite, En – enstatite, Fsp – K-feldspar, Hbl – hornblende, Ol – olivine, Qz – quartz.

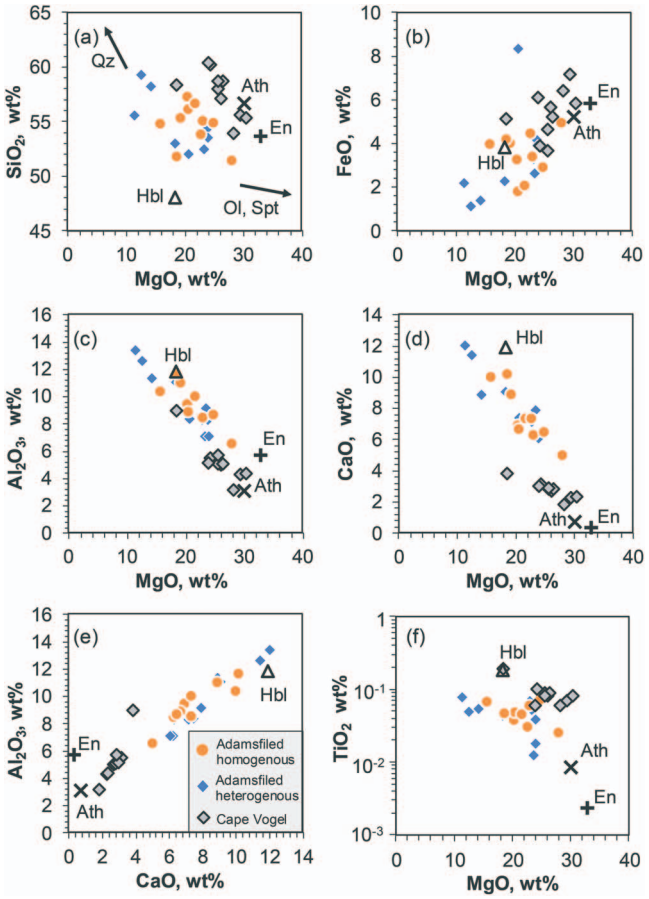

Fig. 9. Major element compositions of completely and partly homogenized inclusions (Table 1). Data on melt inclusions in Cr-spinel from Cape Vogel boninites is from Kamenetsky *et al.* (2002). Typical compositions of minerals comprising unheated inclusions are shown as black markers (Table S3).

assemblages and compositions, the hexagonal outlines of all inclusions adopt the shape of a negative Os monocrystal (Fig. 5). We are also confident that post-crystallization fracturing in the Adamsfield osmium nuggets, which could have provided potential pathways for circulating low-temperature fluids and related modification of already trapped inclusions, had not occurred. This contention is strongly supported by the compositions of the trapped magnesian minerals (olivine and orthopyroxene; Table S3) that are most prone to alteration to serpentine and talc, especially given that their host osmium nuggets originated from serpentinized peridotites nearby (Mertie Jr., 1969). With few exceptions, the inclusions are devoid of serpentine, talc and chlorite. Importantly, this indicates that other, more resistant minerals in the multiphase inclusions apparently escaped low-temperature modifications after entrapment. Finally, unlikely post-entrapment exchange via diffusion of all elements aside from Fe between the entrapped silicate phases and host osmium precludes compositional modification of the entrapped silicates.

The mineral constituents of the multiphase inclusions, such as the quartz-enstatite-hornblende or enstatite-anthophyllite assemblages are atypical of magmatic conditions. Perple_X phase equilibrium modeling did not allow for reproducing the exact observed mineral assemblage (Suppl. Fig. S2); however, broadly similar hornblende and quartz assemblage can be found in the retrogressively metamorphosed mafic (granulite–upper amphibolite to amphibolite facies) of the Adamsfield complex (Mulder *et al.*, 2016). This does not unequivocally suggest an initially metamorphic environment of Os-Ir-Ru alloy crystallization environment—the inclusion could have been captured and then metamorphosed. Simultaneously, the inclusions on a post-entrapment stage may acquire a negative crystal shape, following the mechanism proposed for negative crystal quartz inclusions in garnet (Cesare *et al.*, 2021). Nevertheless, irrespective of their origin, the inclusions remained encapsulated within Os-Ir-Ru alloys, thereby maintaining their overall chemical composition.

Do multiphase inclusions represent trapped melts?

Euhedral olivine ($Fo_{89.3–94.5}$), Cr-spinel, clinopyroxene (Mg# = 0.7–1.0) and orthopyroxene ($En_{84.8–98.2}$) inclusions in Os-Ir-Ru alloy from the Adamsfield and Heazlewood River placers have been interpreted as '…primary minerals, crystallized from a magma that became trapped within the later-formed Os-Ir-Ru alloys' (Peck *et al.*, 1992). Our research confirms the occurrence of previously reported monophase olivine and Cr-spinel inclusions (Fig. 6); however, such seemingly liquidus inclusions are much less abundant compared to the multiphase inclusions reported here (Fig. 5).

The primary and pristine character of the multiphase inclusions could be accounted for if they are regarded as *bona fide* crystallized melt inclusions. Genuine melt inclusions must satisfy the following petrological and mineralogical criteria (e.g. Kamenetsky & Kamenetsky, 2010): (1) the inclusion contents can be homogenized at specific temperatures and pressures to yield a single melt phase; (2) their compositions must be consistent across different zones of a crystal; and (3) glasses produced in heated inclusions should reflect the melt-crystal equilibrium and match natural melt compositions. Half of the inclusions heated at 1400°C satisfied the first criterion, while others contained peritectic or residual crystals of forsterite and enstatite. The second requirement was not met because even for a single grain, the composition of homogenized inclusions is variable (e.g. from 20 to 27 wt % MgO; inclusions 0–1 and 0–4 in Table 1).

A search for natural melt compositions comparable to those of glasses in our heated multiphase inclusions showed that they

Table 1: Composition of inclusions heated at 1400°C

#	Inclusion ID	Na_2O	MgO	Al_2O_3	SiO_2	P_2O_5	Cl	K_2O	CaO	TiO_2	Cr_2O_3	MnO	FeO	Total	Type
1	0–1	0.33	20.32	9.40	57.31	0.00	0.02	0.03	6.88	0.04	0.08	0.16	3.25	97.80	Hom.
2	0–4	0.36	27.85	6.47	51.40	0.04	0.02	0.03	4.97	0.03	0.14	0.09	4.95	96.33	Hom.
3	1–10	0.35	20.64	8.40	52.09	0.01	0.02	0.02	7.42	0.04	0.07	0.11	8.37	97.53	Heter.
4	1–1a	0.35	21.65	9.94	56.67	0.02	0.01	0.03	7.28	0.05	0.04	0.12	2.09	98.24	Hom.
5	1–1b	0.44	19.23	10.93	55.35	0.00	0.02	0.01	8.84	0.04	0.03	0.05	4.03	98.96	Hom.
6	1–8	0.34	22.59	8.50	53.86	0.02	0.01	0.02	7.27	0.03	0.06	0.09	4.45	97.24	Hom.
7	2–10	0.62	18.23	11.08	53.07	0.02	0.00	0.02	9.05	0.04	0.17	0.13	2.33	94.77	Heter.
8	3–3	0.33	23.98	8.19	56.51	0.00	0.01	0.02	6.10	0.02	0.02	0.06	2.38	97.64	Heter.
9	3–4	0.00	36.89	1.12	55.44	0.00	0.00	0.00	0.58	0.01	0.70	0.07	4.04	98.85	Hom.
10	3–8	0.01	53.99	0.00	40.85	0.00	0.00	0.00	0.03	0.00	0.00	0.09	6.27	101.23	Olivine
11	4–3a	1.12	11.27	13.37	55.63	0.00	0.03	0.02	12.01	0.08	0.06	0.06	2.22	95.86	Hom.
12	4–3b	0.62	23.01	8.41	55.08	0.01	0.02	0.04	6.23	0.06	0.01	0.11	3.42	97.02	Hom.
13	4–5a	0.30	23.24	7.12	52.57	0.00	0.01	0.02	6.21	0.05	0.05	0.13	3.31	93.00	Heter.
14	4–5b	0.53	24.77	8.65	54.88	0.04	0.02	0.03	6.42	0.07	0.03	0.12	2.90	98.45	Hom.
15	4–5c	0.31	24.75	7.67	54.46	0.02	0.02	0.02	6.03	0.04	0.05	0.13	3.07	96.55	Hom.
16	4–6	0.54	22.77	8.27	53.83	0.01	0.01	0.05	7.13	0.07	0.18	0.15	4.46	97.48	Heter.
17	4–9	1.25	12.40	12.62	59.38	0.06	0.06	0.15	11.42	0.05	0.05	0.08	1.18	98.68	Hom.
18	5–8a	0.27	24.22	7.50	54.75	0.00	0.01	0.02	5.84	0.01	0.11	0.10	3.46	96.30	Heter.
19	5–8b	0.32	24.54	7.19	53.78	0.00	0.02	0.02	5.76	0.02	0.09	0.13	2.74	94.62	Heter.
20	6–8	0.49	23.77	8.34	54.43	0.04	0.02	0.04	6.29	0.04	0.15	0.10	4.23	97.94	Heter.
21	6–9	0.31	23.83	7.13	53.60	0.02	0.00	0.01	6.07	0.02	0.24	0.13	3.95	95.32	Hom.
22	7–6	0.59	15.71	10.30	54.78	0.03	0.01	0.03	9.97	0.07	0.11	0.13	3.98	95.71	Hom.
23	7–9	1.12	14.12	11.32	58.27	0.02	0.03	0.29	8.87	0.06	0.02	0.08	1.42	95.63	Heter.
24	8–1	0.57	20.44	8.82	56.11	0.00	0.35	0.81	6.65	0.05	0.13	0.11	1.78	95.82	Hom.
25	8–2	0.22	23.44	9.17	54.01	0.01	0.00	0.02	7.89	0.01	0.10	0.13	2.67	97.68	Heter.
26	8–4	0.62	18.58	11.56	51.81	0.02	0.02	0.01	10.12	0.05	0.02	0.09	4.21	97.11	Hom.
27	8–9	0.12	24.14	5.32	54.46	0.00	0.01	0.01	4.30	0.02	0.07	0.10	4.95	93.51	Heter.

Note: The complete dataset is available in Supplementary Table S1. Type: 'Hom.' refers to fully homogenized inclusions, and 'heter.' refers to inclusions containing peritectic crystals

tentatively correspond to low-Ca boninite types (Fig. 9). Although some high-Mg, high-Si and low-Ti glass compositions can be viewed as marginally close to the boninitic melt, other components, most of all Al_2O_3 and CaO, do not match boninites. Moreover, the highly variable major element compositions of glasses (Fig. 9) and mineral inclusions ($Fo_{89.3–94.5}$, $En_{84.8–98.2}$) require the inclusions (hence, host osmium) to have formed from melts of strongly different compositions. The crystallization of compositionally narrow Os-Ir-Ru alloys from different melts is unrealistic, since fractional crystallization leads to strong change in melt PGE content (Dale *et al.*, 2012).

Alternatively, the observed compositional variations in the experimental glasses (Fig. 9), and a variety of crystalline phases in the multiphase inclusions (Fig. 5), may instead represent a heterogeneous parental media (e.g. mixture of melt and micrometer-scale crystals—'crystal mush') of Os-Ir-Ru. The 'crystal mush' environment may account for both the inhomogeneity in phase assemblage and major element chemistry of the multiphase inclusions that are hardly homogenized even at 1400°C, which is unrealistically high for the crustal conditions. Entrapment of Ca- and Al-rich hornblende and Mg-rich minerals, allegedly occurring in different proportions during the growth of the host Os-Ir-Ru alloy, is supported by the observed positive correlations between CaO and Al_2O_3 in the experimental glasses (Fig. 9e) and the negative correlation between these components and MgO (Fig. 9c, d).

A magmatic scenario of the nugget's origin should consider a mass-balance between the source of Os and Ir and the size of the nugget. Based on simple calculations, ~18 m^3 of basaltic melt with 0.4 ppb Os + Ir (a reasonable concentration for arc magmas (Park *et al.*, 2017, Kutyrev *et al.*, 2021a)) and a density of 2.8 g/cm^3 is required to form a 1-mm spherical grain (~10 mg Os, assuming 50% metal extraction) typical for ophiolite-related placers (e.g. Cabri *et al.*, 2022). Furthermore, ~125 500 m^3 of melt would be required to continuously crystallize the largest Os-Ir-Ru nugget reported in Tasmania (70 g, 3.1 cm^3, Reid, 1921). In sulfide-saturated systems, a high silicate/sulfide ratio is responsible for accumulation of PGE (e.g. Campbell & Naldrett, 1979); however, there are no equivalent models for sulfide-free systems. For example, the empirical partition coefficient $D^{Cr\text{-}spinel\text{-}silicate\ melt}$ for Os does not exceed 280 (Park *et al.*, 2017), which is several orders of magnitude lower than $D^{sulfide\text{-}silicate\ melt}$ values (Mungall & Brenan, 2014).

Previously, micrometer-scale grains of Os-Ir-Ru alloys have been reported in volcanic rocks (Kamenetsky *et al.*, 2015; Locmelis *et al.*, 2018). It may be speculated that larger grains (10–100 μm) can crystallize from the melt and accumulate together with Cr-spinel; however, the proportion of PGM in this case will be negligible compared to Cr-spinel, i.e. this mechanism could account for a formation of a moderately PGE-enriched chromitite (like in many layered intrusions, e.g. Oberthür *et al.*, 2015) but still inapplicable in the case of a high chromite tenor, e.g. occurrence of Pt-Fe nuggets in chromitites of the Ural-Alaskan-type complexes (Augé *et al.*, 2005).

Another possibility is growth of a static grain during the formation of chromitite by melt percolation through mantle peridotites (Kelemen, 1990; Arai, 1997; González-Jiménez *et al.*, 2014b). However, such growth of Os-Ir-Ru still requires a very large volume of melt (see mass-balance calculations above) to pass through a narrow conduit. Additionally, such melt should be silica-rich (~57 wt % SiO_2 as in the most evolved inclusions, Fig. 9a) and crystallize hornblende and quartz that coexist with high-Mg olivine as

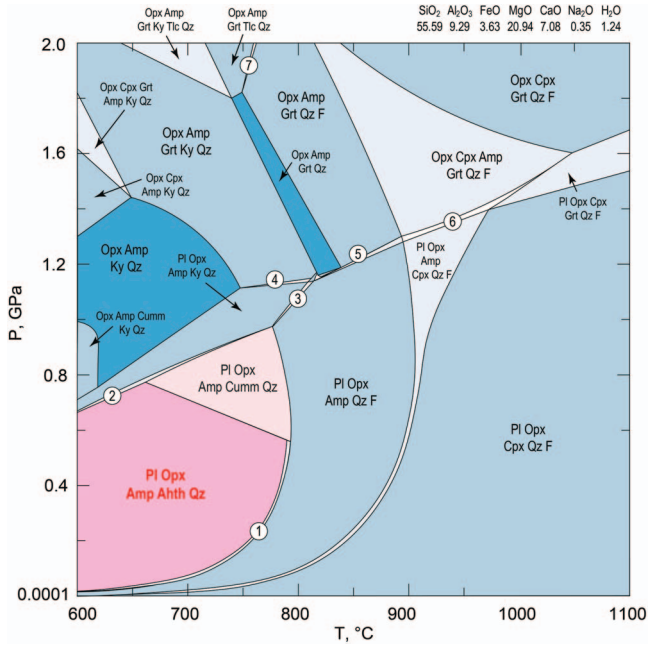

Fig. 10. Phase diagram for the composition of the average inclusion quantified using PERPLE_X software (Connolly, 2005). The paragenesis Pl-Opx-Amp-Ath-Qz is appropriate to the 'average' inclusion. Abbreviations: Pl – plagioclase, Opx – orthopyroxene, Cpx – clinopyroxene, Grt – garnet, Amp – amphibole, Cum – cummingtonite, Ath – anthophyllite, Ky – kyanite, Qz – quartz, Tlc – talc, F – water fluid. (1 – Pl-Opx- Ath-Amp-Qz-F, 2 – Fsp-Opx- Ath-Amp-Ky-Qz, 3 – Fsp-Opx-Amp-Ky-Qz-F, 4 – Fsp-Grt-Opx-Amp-Ky-Qz, 5 – Fsp-Grt-Opx-Amp-Qz-F, 6 – Fsp-Grt-Opx-Cpx-Amp-Qz-F, 7 – Opx-Grt-Amp-Tlc-Qz-F).

recorded in the studied inclusions (Fig. 5a). Overall, this scenario is improbable.

Multi-stage origin of the nuggets

Magmatic models discussed above can account for the origin of small PGM disseminated in chromitites. However, due to the mass-balance problems, none of these models can explain the origin of large nuggets and the inclusions observed. If the initial accumulation of PGE was driven by the magmatic processes (accumulation as admixture in Cr-spinel, magmatic PGM or sulfides), redistribution and further accumulation of Os may occur in essentially non-magmatic conditions:

1) Desulfidation of early (e.g. magmatic) sulfide due to the interaction with sulfur-undersaturated melt or oxidizing fluids leading to the formation of Os-Ir-Ru alloys in mantle peridotites (Luguet *et al.*, 2007; Fonseca *et al.*, 2012; Prichard *et al.*, 2017) and PGM nuggets in crustal mafic–ultramafic rocks (Naldrett & von Gruenewaldt, 1989). This process may be effective in PGE accumulation: dissolution of 1 kg of pentlandite comprising 100 ppm Os and 100 ppm Ir (reasonable concentration for pentlandite, Mansur *et al.*, 2020) will provide Os-Ir-Ru alloy grain of 0.2 g. However, in the case of Adamsfield, no relict base metal sulfide inclusions are present, indicating that either the sulfide dissolution was complete, or that the sulfides did not play a significant role in this case.

2) Relatively low-temperature processes, such as serpentinization, can lead to PGE alloys precipitation from reduced fluids, as has been demonstrated in limited studies of natural samples (Dmitrenko & Mochalov, 1989; Evans *et al.*, 2023; Kutyrev *et al.*, 2023). Alteration/re-equilibration cycles in peridotite have been shown to trigger multiple dissolution-precipitation events, consequently leading to the formation of relatively large nuggets from minute PGM grains (González-Jiménez *et al.*, 2014a).

3) Osmium transport and precipitation in supercritical oxidized brines in upper mantle/lower crust conditions (Foustoukos, 2019), pointing to direct growth of Os-Ir-Ru from high-temperature metamorphic fluids. So far, there is clear evidence of Os being transported in volcanic fluids, most likely as chloro complexes (Distler *et al.*, 2008; Yudovskaya *et al.*, 2008). Although comprehensive data on the solubility of osmium in these fluids is lacking (Xiong & Wood, 2000), current understanding highlights the formation of volatile aqueous oxidized Os species under oxidizing conditions (ΔQFM+5) at temperatures above 850°C (Foustoukos, 2019). Experimental findings also underscore the role of slab-derived fluids in producing elevated Os/Ir ratios in metasomatized xenoliths compared to the primitive upper mantle. This is attributed to the enhanced mobility of osmium in the form of chlorine and oxygen-bearing volatile aqueous complexes (Distler *et al.*, 2008; Yudovskaya *et al.*, 2008; Foustoukos, 2019; Yan *et al.*, 2022).

4) Mechanical accumulation of solid particles in high-*T* post-magmatic liquids (Pushkarev *et al.*, 2007). This model suggests that after solidification and compaction of a cumulate pile, there is intergranular melt enriched in volatiles, Ca, alkalis, Cr-spinel and PGM crystals. As the crystal pile ascends and pressure lowers, this melt exsolves fluids that accumulates Cr-spinel, as was experimentally shown by Matveev & Ballhaus (2002), and, presumably, PGM. Subsequently, fractures and cavities become filled with Cr-spinels, PGM and hydrous silicates crystallized from residual melt. Because temperatures are still close to magmatic, this mass soon equilibrates with the surrounding peridotite, forming podiform chromitite.

Each of the above cited mechanisms have a potential of explaining the origin of nuggets through the involvement of post-magmatic or metamorphic fluids. Because the studied grains originate from an outcrop of metamorphosed oceanic crust, including upper mantle sections, it may be suggested that the origin of the mineralization is a consequence of a series of events accompanying the history of a typical ophiolite. This includes: (a) partial melting of a mantle source, (b) magmatic accumulation, (c) high-temperature deformations, (d) percolation of interstitial melts and subsolidus fluids, (e) low-temperature alteration and (f) metamorphism (both pro- and retrograde). Moreover, some events can be repetitive, i.e. serpentinized peridotite may be assimilated or react with novel portions of melt. This scenario was used to explain heterogenous multiphase inclusions in Cr-spinel from Oman ophiolite (Borisova *et al.*, 2012). According to this model, in the initial stage, a mantle protolith altered by seawater-derived hydrothermal fluids produced serpentinites and serpentinized harzburgites, which were the primary sources of chromium for chromitite ore and account for the systematically high Mg/Fe ratios in the silicate minerals present in the ophiolite chromitites.

The sequence of osmium crystallization could be represented as follows (Fig. 11):

1) Initial magmatic crystallization and accumulation, including silicates, Cr-spinel, minute Os-Ir-Ru alloy crystals and sulfides, if oxygen/sulfur fugacity permits.

2) High-temperature (near solidus) post-magmatic processes. This stage may include mobilization and accumulation of magmatic PGM and Cr-spinels, followed by equilibration with the hot crystal pile (Matveev & Ballhaus, 2002; Pushkarev *et al.*, 2007).

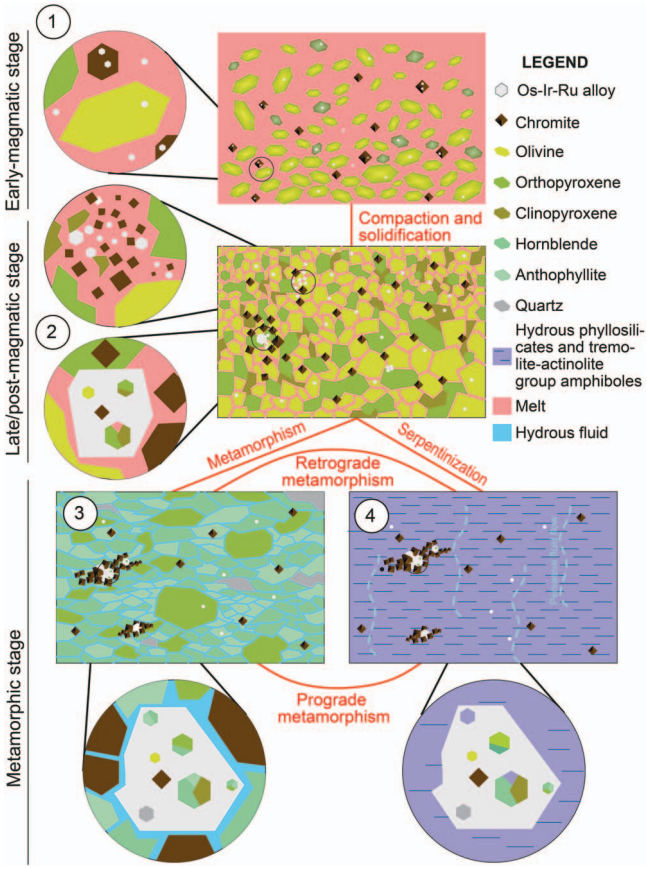

Fig. 11. The multistage model of Os-Ir-Ru nuggets formation. The process begins with (1) the magmatic crystallization and accumulation of silicates, Cr-spinel, minute Os-Ir-Ru alloy crystals and sulfides, if oxygen/sulfur fugacity permits (sulfides not shown for simplicity). Subsequently, (2) high-temperature (near solidus) post-magmatic processes induce mobilization and accumulation of magmatic PGM and Cr-spinels, followed by equilibration with the hot crystal pile (Matveev & Ballhaus, 2002; Pushkarev *et al.*, 2007). The following relatively low-temperature modification (3) includes serpentinization and other types of retrograde metamorphism, accompanied by PGE accumulation through potential desulfidation and/or redeposition of earlier alloy PGM. Prograde metamorphism of the altered mineralized ultramafic rocks (4), caused by either tectonic processes or interaction with new magma portions. Prograde and retrograde metamorphic episodes may cyclically interchange one another depending on the individual tectonic history of a complex. See the text for further details.

3) Relatively low-temperature modification. This includes serpentinization and other types of metamorphism, accompanied by PGE accumulation through potential desulfidation and/or redeposition of earlier alloy PGM.

4) Higher grade metamorphism of the altered mineralized ultramafic rocks, caused by either tectonic processes or interaction with new magma portions (i.e. melt/serpentinite interaction as proposed by Borisova *et al.* (2012).

5) Repetition of stage 3 during the exhumation of an ultramafic complex.

The proposed origin of osmium in a sequence of magmatic and metamorphic events agrees with the mineralogical observations, such as coexistence within a single Os-Ir-Ru of quartz and high-Mg olivine inclusions—minerals that cannot co-precipitate under thermodynamic equilibrium conditions but still are hosted by the same grain of Os-Ir-Ru (Fig. 5a). We interpret such occurrences as a result of a prolonged series of events when olivine was captured at the early (magmatic?) stage and protected by growing osmium from interaction with later melts or fluids. Where olivine was captured at the metamorphic stage, it exhibits zonation with Fe-rich outer layers and is enveloped by hornblende and chlorite (Fig. 5g). An intergrowth of hornblende and Cr-spinel within this inclusion demonstrates that Cr-spinel can crystallize in a proposed metamorphic setting. The assemblage of hornblende, quartz, anthophyllite, chlorite, etc., in our study represents the parental metamorphic media of Os-Ir-Ru growth.

The extended metamorphic equilibration obliterated the zonation in Os-Ir-Ru alloys, rendering the grains their current homogeneous appearance. Only the inclusions retain evidence of their prolonged formation history. Simultaneously, a negative crystal shape may be acquired by the inclusions on a post-entrapment stage, driven by the minimization of the surface energy of the host-inclusion system as it has been shown for quartz inclusions in garnet (Cesare *et al.*, 2021).

Multi-stage processes are further supported by the heterogenous $^{187}Os/^{188}Os$ in dunites and chromitites of the same ultramafic complexes (Shi *et al.*, 2007; González-Jiménez *et al.*, 2013). Theoretically, these stages may be paralleled with the supra-subduction zone ophiolites' staged lifecycle that includes birth, youth, maturity, death and resurrection (Shervais, 2001), including both magmatic and metamorphic processes. Therefore, what initially appears as a product of a singular, uniform event is, in fact, a result of a punctuated sequence of events, including melt-fluid–rock interaction and metasomatic alteration, all ultimately superseded by a concluding metamorphic transformation.

CONCLUSIONS

Our findings challenge the existing paradigm of direct single-stage large PGM nuggets' crystallization from boninitic or any other magmatic melt. Instead, we propose an intricate multi-stage genesis for these nuggets, wherein the repeated occurrence of distinct stages plays a pivotal role in their development. This complex scenario, founded on primary multiphase inclusions, reveals a story of interchanging magmatic and metamorphic processes, all contributing to the concentration of osmium. By inference, similar processes should be considered in understanding origin of podiform chromitites and their host dunites.

ACKNOWLEDGEMENTS

We are grateful to Prof David H. Green for his assistance in getting access to Adamsfield samples. This work was supported by the Visiting Scientist Award by the Chinese Academy of Sciences (V.S.K.). The research was partially conducted in the Research Centre for X-ray Diffraction Studies and in the 'Geomodel' Research Centre of St. Petersburg State University (state registration number AAAA-A19-119091190094-6). The high-temperature experiments using a gas-mixing tube furnace were carried out within the State Assignment of Vernadsky Institute framework (S.P.K.). Additional experiments were fulfilled under Research program FMUF-2022-0004 of the D.S. Korzhinskii Institute of Experimental Mineralogy RAS (I.F.C.). This work is Cardiff EARTH CRediT Contribution 25. The assistance of Maya Kamenetsky is warmly acknowledged. This paper benefited from thoughtful comments by Michael Anenburg, Anastassia Borisova, anonymous reviewer and editors Georg Zellmer and Reto Gieré. The work of Katy Evans, Andrew Tomkins, and Chris Ballhaus, who reviewed the early version of this manuscript, is kindly acknowledged.

DATA AVAILABILITY

The data underlying this article are available in the article and in its online supplementary material.

SUPPLEMENTARY DATA

Supplementary data are available at Journal of Petrology online.

CONFLICT OF INTEREST

The authors declare that they have no known competing financial interests or personal relationships that could have appeared to influence the work reported in this paper.

REFERENCES

Anenburg, M. & Mavrogenes, J. A. (2016). Experimental observations on noble metal nanonuggets and Fe-Ti oxides, and the transport of platinum group elements in silicate melts. *Geochimica et Cosmochimica Acta* **192**, 258–278. https://doi.org/10.1016/j.gca.2016.08.010.

Apopei, A. I. & Buzgar, N. (2010). The Raman study of amphiboles. *Analele Ştiinţifice ale Universităţii Al. I. Cuza Iaşi, Geologie* **56**(1), 57–83.

Arai, S. (1997). Origin of podiform chromitites. *Journal of Asian Earth Sciences* **15**, 303–310. https://doi.org/10.1016/S0743-9547(97)00015-9.

Arai, S. & Akizawa, N. (2014). Precipitation and dissolution of chromite by hydrothermal solutions in the Oman ophiolite: new behavior of Cr and chromite. *American Mineralogist* **99**, 28–34. https://doi.org/10.2138/am.2014.4473.

Augé, T., Genna, A., Legendre, O., Ivanov, K. S. & Volchenko, Y. A. (2005). Primary platinum mineralization in the Nizhny Tagil and Kachkanar ultramafic complexes, Urals, Russia: a genetic model for PGE concentration in chromite-rich zones. *Economic Geology* **100**, 707–732. https://doi.org/10.2113/gsecongeo.100.4.707.

Barnes, S. J., Naldrett, A. J. & Gorton, M. P. (1985). The origin of the fractionation of platinum-group elements in terrestial magmas. *Chemical Geology* **53**, 303–323. https://doi.org/10.1016/0009-2541(85)90076-2.

Borg, G. & Hattori, K. (1997). Evolution of PGE-mineralization of the Nishni Tagil ultramafic complex, Urals – genetic constraints from Os-isotope and SEM studies.

Borisova, A. Y., Ceuleneer, G., Kamenetsky, V. S., Arai, S., Béjina, F., Abily, B., Bindeman, I. N., Polvé, M., De Parseval, P., Aigouy, T. & Pokrovski, G. S. (2012). A new view on the petrogenesis of the Oman ophiolite chromitites from microanalyses of chromite-hosted inclusions. *Journal of Petrology* **53**, 2411–2440. https://doi.org/10.1093/petrology/egs054.

Cabri, L. J. & Harris, D. C. (1975). Zoning in Os-Ir alloys and the relation of the geological and tectonic environment of the source rocks to the bulk Pt:Pt+Ir+Os ratio for placers. *Canadian Mineralogist* **13**, 266–274.

Cabri, L. J., Oberthür, T. & Keays, R. R. (2022). Origin and depositional history of platinum-group minerals in placers – a critical review of facts and fiction. *Ore Geology Reviews*. **144**, 104733. https://doi.org/10.1016/j.oregeorev.2022.104733.

Calver, C. R., Everard, J. L., Berry, R. F., Bottrill, R. S. & Seymour, D. B. (2014) Proterozoic Tasmania. In: Corbett K. D., Quilty P. G. & Calver C. R. (eds) *Geological Evolution of Tasmania*. Sydney, Australai: Gegological Society of Australia.

Campbell, I. H. & Naldrett, A. J. (1979). The influence of silicate:sulfide ratios on the geochemistry of magmatic sulfides. *Economic Geology* **74**, 1503–1506. https://doi.org/10.2113/gsecongeo.74.6.1503.

Cesare, B., Parisatto, M., Mancini, L., Peruzzo, L., Franceschi, M., Tacchetto, T., Reddy, S., Spiess, R., Nestola, F. & Marone, F. (2021). Mineral inclusions are not immutable: evidence of post-entrapment thermally-induced shape change of quartz in garnet. *Earth and Planetary Science Letters* **555**, 116708. https://doi.org/10.1016/j.epsl.2020.116708.

Chayka, I. F., Kamenetsky, V. S., Malitch, K. N., Vasil'ev, Y. R., Zelenski, M. E., Abersteiner, A. B. & Kuzmin, I. A. (2023). Behavior of critical metals in cumulates of alkaline ultramafic magmas in the Siberian large igneous province: insights from melt inclusions in minerals. *Ore Geology Reviews* **160**, 105577. https://doi.org/10.1016/j.oregeorev.2023.105577.

Connolly, J. A. D. (2005). Computation of phase equilibria by linear programming: a tool for geodynamic modeling and its application to subduction zone decarbonation. *Earth and Planetary Science Letters* **236**, 524–541. https://doi.org/10.1016/j.epsl.2005.04.033.

Crawford, A. J. & Berry, R. F. (1992). Tectonic implications of Late Proterozoic-Early Palaeozoic igneous rock associations in western Tasmania. *Tectonophysics* **214**, 37–56. https://doi.org/10.1016/0040-1951(92)90189-D.

Dale, C. W., Macpherson, C. G., Pearson, D. G., Hammond, S. J. & Arculus, R. J. (2012). Inter-element fractionation of highly siderophile elements in the Tonga Arc due to flux melting of a depleted source. *Geochimica et Cosmochimica Acta* **89**, 202–225. https://doi.org/10.1016/j.gca.2012.03.025.

Distler, V. V., Dikov, Y. P., Yudovskaya, M. A., Chaplygin, I. V. & Buleev, M. I. (2008). Platinum-chlorine-phosphorus-hydrocarbon complex in volcanic fluids: the first find in the terrestrial environment. *Doklady Earth Sciences* **420**, 628–631. https://doi.org/10.1134/S1028334X08040223.

Dmitrenko, G. G. & Mochalov, A. G. (1989). Origin of hydrous silicate inclusions in PGM and Cr-spinels from ultramafic rocks. *Doklady Akademii Nauk SSSR* **307**, 1207–1211.

Evans, K. A., Frost, B. R., Reddy, S. M. & Brown, T. C. (2023). Causes, effects, and implications of the relationships amongst fluids, serpentinisation, and alloys. *Lithos* **446-447**, 107132. https://doi.org/10.1016/j.lithos.2023.107132.

Finnigan, C. F., Brennan, J. M., Mungall, J. E. & McDonough, W. F. (2008). Experiments and models bearing on the role of chromite as a collector of platinum group minerals by local reduction. *Journal of Petrology* **49**, 1647–1665. https://doi.org/10.1093/petrology/egn041.

Fonseca, R. O. C., Laurenz, V., Mallmann, G., Luguet, A., Hoehne, N. & Jochum, K. P. (2012). New constraints on the genesis and long-term stability of Os-rich alloys in the Earth's mantle. *Geochimica et Cosmochimica Acta* **87**, 227–242. https://doi.org/10.1016/j.gca.2012.04.002.

Ford, R. J. (1981). Platinum-group minerals in Tasmania. *Economic Geology* **76**, 498–504. https://doi.org/10.2113/gsecongeo.76.2.498.

Foustoukos, D. I. (2019). Hydrothermal oxidation of Os. *Geochimica et Cosmochimica Acta* **255**, 237–246. https://doi.org/10.1016/j.gca.2019.04.019.

Fuhrman, M. & Lindsley, D. H. (1988). Ternary-feldspar modeling and thermometry. *American Mineralogist* **73**, 201–215.

González-Jiménez, J. M., Marchesi, C., Griffin, W. L., Gutiérrez-Narbona, R., Lorand, J.-P., O'Reilly, S. Y., Garrido, C. J., Gervilla, F., Pearson, N. J. & Hidas, K. (2013). Transfer of Os isotopic signatures from peridotite to chromitite in the subcontinental mantle: insights from in situ analysis of platinum-group and base-metal minerals

(Ojén peridotite massif, southern Spain). *Lithos* **164-167**, 74–85. https://doi.org/10.1016/j.lithos.2012.07.009.

González-Jiménez, J. M., Griffin, W. L., Gervilla, F., Proenza, J. A., O'Reilly, S. Y. & Pearson, N. J. (2014a). Chromitites in ophiolites: how, where, when, why? Part I. A review and new ideas on the origin and significance of platinum-group minerals. *Lithos* **189**, 127–139. https://doi.org/10.1016/j.lithos.2013.06.016.

González-Jiménez, J. M., Griffin, W. L., Proenza, J. A., Gervilla, F., O'Reilly, S. Y., Akbulut, M., Pearson, N. J. & Arai, S. (2014b). Chromitites in ophiolites: how, where, when, why? Part II. The crystallization of chromitites. *Lithos* **189**, 140–158. https://doi.org/10.1016/j.lithos.2013.09.008.

Green, E. C. R., White, R. W., Diener, J. F. A., Powell, R., Holland, T. J. B. & Palin, R. M. (2016). Activity–composition relations for the calculation of partial melting equilibria in metabasic rocks. *Journal of Metamorphic Geology* **34**, 845–869. https://doi.org/10.1111/jmg.12211.

Harris, D. C. & Cabri, L. J. (1991). Nomenclature of platinum-group-element alloys: review and revision. *The Canadian Mineralogist* **29**, 231–237.

Hiemstra, S. A. (1979). The role of collectors in the formation of the platinum deposits in the Bushveld Complex. *The Canadian Mineralogist* **17**, 469–482.

Holland, T. J. B. & Powell, R. (2011). An improved and extended internally consistent thermodynamic dataset for phases of petrological interest, involving a new equation of state for solids. *Journal of Metamorphic Geology* **29**, 333–383. https://doi.org/10.1111/j.1525-1314.2010.00923.x.

Kamenetsky, V. S. & Kamenetsky, M. B. (2010). Magmatic fluids immiscible with silicate melts: examples from inclusions in phenocrysts and glasses, and implications for magma evolution and metal transport. *Geofluids* **10**, 293–311. https://doi.org/10.1111/j.1468-8123.2009.00272.x.

Kamenetsky, V. S., van Achterbergh, E., Ryan, C. G., Naumov, V. B., Mernagh, T. P. & Davidson, P. (2002). Extreme chemical heterogeneity of granite-derived hydrothermal fluids: an example from inclusions in a single crystal of miarolitic quartz. *Geology* **30**, 459–462. https://doi.org/10.1130/0091-7613(2002)030<0459:ECHOGD>2.0.CO;2.

Kamenetsky, V. S., Park, J. W., Mungall, J. E., Pushkarev, E. V., Ivanov, A. V., Kamenetsky, M. B. & Yaxley, G. M. (2015). Crystallization of platinum-group minerals from silicate melts: evidence from Cr-spinel-hosted inclusions in volcanic rocks. *Geology* **43**, 903–906. https://doi.org/10.1130/G37052.1.

Kelemen, P. B. (1990). Reaction between ultramafic rock and fractionating basaltic magma I. Phase relations, the origin of calc-alkaline magma series, and the formation of discordant Dunite. *Journal of Petrology* **31**, 51–98. https://doi.org/10.1093/petrology/31.1.51.

Krasheninnikov, S. P., Sobolev, A. V., Batanova, V. G., Kargaltsev, A. A. & Borisov, A. A. (2017). Experimental testing of olivine–melt equilibrium models at high temperatures. *Doklady Earth Sciences* **475**, 919–922. https://doi.org/10.1134/s1028334x17080153.

Kutyrev, A. V., Sidorov, E. G., Antonov, A. V. & Chubarov, V. M. (2018). Platinum-group mineral assemblage of the Prizhimny Creek (Koryak Highland). *Russian Geology and Geophysics* **59**, 935–944. https://doi.org/10.1016/j.rgg.2018.07.014.

Kutyrev, A. V., Kamenetsky, V. S., Sidorov, E. G., Abersteiner, A. & Chubarov, V. M. (2020). Silicate inclusions in isoferroplatinum: constraints on the origin of platinum mineralization in podiform chromitites. *Ore Geology Reviews* **119**, 103367–103313. https://doi.org/10.1016/j.oregeorev.2020.103367.

Kutyrev, A. V., Kamenetsky, V. S., Park, J.-W., Maas, R., Demonterova, E. I., Antsiferova, T. N., Ivanov, A. V., Hwang, J., Abersteiner, A. & Ozerov, A. Y. (2021a). Primitive high-K intraoceanic arc magmas of Eastern Kamchatka: implications for Paleo-Pacific tectonics and magmatism in the Cretaceous. *Earth-Science Reviews* **220**, 103703–103722. https://doi.org/10.1016/j.earscirev.2021.103703.

Kutyrev, A. V., Sidorov, E. G., Kamenetsky, V. S., Chubarov, V. M., Chayka, I. F. & Abersteiner, A. (2021b). Platinum mineralization and geochemistry of the Matysken zoned Ural-Alaskan type complex and related placer (Far East Russia). *Ore Geology Reviews* **130**, 1–17. https://doi.org/10.1016/j.oregeorev.2020.103947.

Kutyrev, A., Kamenetsky, V. S., Kontonikas-Charos, A., Savelyev, D. P., Yakich, T. Y., Belousov, I. A., Sandimirova, E. I. & Moskaleva, S. V. (2023). Behavior of platinum-group elements during hydrous metamorphism: constraints from awaruite (Ni3Fe) mineralization. *Lithosphere* **2023**. https://doi.org/10.2113/2023/lithosphere_2023_126.

Latypov, R. M., Chistyakova, S. Y., Namur, O. & Barnes, S. (2020). Dynamics of evolving magma chambers: textural and chemical evolution of cumulates at the arrival of new liquidus phases. *Earth-Science Reviews* **210**, 103388. https://doi.org/10.1016/j.earscirev.2020.103388.

Locmelis, M., Fiorentini, M. L., Barnes, S. J., Hanski, E. J. & Kobussen, A. F. (2018). Ruthenium in chromite as indicator for magmatic sulfide liquid equilibration in mafic-ultramafic systems. *Ore Geology Reviews* **97**, 152–170. https://doi.org/10.1016/j.oregeorev.2018.05.002.

Luguet, A., Shirey, S. B., Lorand, J.-P., Horan, M. F. & Carlson, R. W. (2007). Residual platinum-group minerals from highly depleted harzburgites of the Lherz massif (France) and their role in HSE fractionation of the mantle. *Geochimica et Cosmochimica Acta* **71**, 3082–3097. https://doi.org/10.1016/j.gca.2007.04.011.

Maier, W. D., Barnes, S.-J. & Groves, D. (2013). The Bushveld Complex, South Africa: formation of platinum–palladium, chrome- and vanadium-rich layers via hydrodynamic sorting of a mobilized cumulate slurry in a large, relatively slowly cooling, subsiding magma chamber. *Mineralium Deposita* **48**, 1–56. https://doi.org/10.1007/s00126-012-0436-1.

Mansur, E. T., Barnes, S.-J. & Duran, C. J. (2020). An overview of chalcophile element contents of pyrrhotite, pentlandite, chalcopyrite, and pyrite from magmatic Ni-Cu-PGE sulfide deposits. *Mineralium Deposita* **56**, 179–204. https://doi.org/10.1007/s00126-020-01014-3.

Matveev, S. & Ballhaus, C. (2002). Role of water in the origin of podiform chromitite deposits. *Earth and Planetary Science Letters* **203**, 235–243. https://doi.org/10.1016/S0012-821X(02)00860-9.

Mertie, J. B., Jr. (1969) *Economic Geology of the Platinum Group Metals*. United States Goverment Printing Office, Washington.

Morgan, G. B. & London, D. (1996). Optimizing the electron microprobe analysis of hydrous alkali aluminosilicate glasses. *American Mineralogist* **81**, 1176–1185. https://doi.org/10.2138/am-1996-9-1016.

Mulder, J. A., Berry, R. F., Meffre, S. & Halpin, J. A. (2016). The metamorphic sole of the western Tasmanian ophiolite: new insights into the Cambrian tectonic setting of the Gondwana Pacific margin. *Gondwana Research* **38**, 351–369. https://doi.org/10.1016/j.gr.2015.12.010.

Mungall, J. E. & Brenan, J. M. (2014). Partitioning of platinum-group elements and Au between sulfide liquid and basalt and the origins of mantle-crust fractionation of the chalcophile elements. *Geochimica et Cosmochimica Acta* **125**, 265–289. https://doi.org/10.1016/j.gca.2013.10.002.

Naldrett, A. (2004) *Magmatic Sulfide Deposits*. New York: Springer.

Naldrett, A. J. & von Gruenewaldt, G. (1989). Association of platinum-group elements with chromitite in layered intrusions and

ophiolite complexes. *Economic Geology* **84**, 180–187. https://doi.org/10.2113/gsecongeo.84.1.180.

Oberthür, T., Junge, M., Rudashevsky, N., de Meyer, E. & Gutter, P. (2015). Platinum-group minerals in the LG and MG chromitites of the eastern Bushveld Complex, South Africa. *Mineralium Deposita* **51**, 71–87. https://doi.org/10.1007/s00126-015-0593-0.

Okrugin, A. V. (2011). Origin of platinum-group minerals from dispersed elements to nuggets in mafic-ultramafic intrusive rocks. *The Canadian Mineralogist* **49**, 1397–1412. https://doi.org/10.3749/canmin.49.6.1397.

Orlov, V. N. (2019). Platinum nuggets from the diamond fund of the Russian Federation: witnesses of history. *Mineralogical Alamanac* **15**, 4–28.

Oshin, I. O. & Crocket, J. H. (1982). Noble metals in Thetford Mines ophiolites, Quebec, Canada; Part I, Distribution of gold, iridium, platinum, and palladium in the ultramafic and gabbroic rocks. *Economic Geology* **77**, 1556–1570. https://doi.org/10.2113/gsecongeo.77.6.1556.

Park, J. W., Kamenetsky, V., Campbell, I., Park, G., Hanski, E. & Pushkarev, E. (2017). Empirical constraints on partitioning of platinum group elements between Cr-spinel and primitive terrestrial magmas. *Geochimica et Cosmochimica Acta* **216**, 393–416. https://doi.org/10.1016/j.gca.2017.05.039.

Peck, D. & Keays, R. R. (1990). Insights into the behavior of precious metals in primitive, S-undersaturated magmas: evidence from the Heazlewood River Complex, Tasmania. *The Canadian Mineralogist* **28**, 553–577.

Peck, D. C., Keays, R. R. & Ford, R. J. (1992). Direct crystallization of refractory platinum-group element alloys from boninitic magmas: evidence from Western Tasmania. *Australian Journal of Earth Sciences* **39**, 373–387. https://doi.org/10.1080/08120099208728031.

Prichard, H. M., Barnes, S. J., Dale, C. W., Godel, B., Fisher, P. C. & Nowell, G. M. (2017). Paragenesis of multiple platinum-group mineral populations in Shetland ophiolite chromitite: 3D X-ray tomography and in situ Os isotopes. *Geochimica et Cosmochimica Acta* **216**, 314–334. https://doi.org/10.1016/j.gca.2017.03.035.

Pushkarev, E. V., Anikina, E. V., Garuti, G. & Zaccarini, F. (2007). Chromium-platinum deposits of Nizhny-Tagil type in the Urals: structural-substantial characteristic and a problem of genesys. *Litosfera* **92**, 28–65.

Reid, A. M. (1921) Osmiridium in Tasmania. *Geological Survey Bulletin* **32**, 1–123.

Seymour, D. B. (2007). *The geology and mineral deposits of Tasmania: a summary/by D.B. Seymour, G.R. Green and C.R. Calver*. Rosny Park, Tas: Dept. of Infrastructure, Energy and Resources.

Shervais, J. W. (2001). Birth, death, and resurrection: the life cycle of suprasubduction zone ophiolites. *Geochemistry, Geophysics, Geosystems* **2**. https://doi.org/10.1029/2000GC000080.

Shi, R., Alard, O., Zhi, X., O'Reilly, S. Y., Pearson, N. J., Griffin, W. L., Zhang, M. & Chen, X. (2007). Multiple events in the Neo-Tethyan oceanic upper mantle: evidence from Ru–Os–Ir alloys in the Luobusa and Dongqiao ophiolitic podiform chromitites, Tibet. *Earth and Planetary Science Letters* **261**, 33–48. https://doi.org/10.1016/j.epsl.2007.05.044.

Smith, W. D. & Maier, W. D. (2021). The geotectonic setting, age and mineral deposit inventory of global layered intrusions. *Earth-Science Reviews* **220**, 103736. https://doi.org/10.1016/j.earscirev.2021.103736.

Stepanov, S. Y., Palamarchuk, R. S., Antonov, A. V., Kozlov, A. V., Valrlamov, D. A., Khanin, D. A. & Zolotarev, A. A., Jr. (2020). Morphology, composition, and ontogenesis of platinum-group minerals in chromitites of zoned clinopyroxenite-dunite massifs of the Middle Urals. *Russian Geology and Geophysics* **61**, 47–67. https://doi.org/10.15372/rgg2019089.

Tolstykh, N. D., Sidorov, E. G. & Kozlov, A. P. (2004). Platinum-group minerals in lode and placer deposits associated with the Ural-Alaskan-type Gal'moenan complex, Koryak Kamchatka Platinum Belt, Russia. *The Canadian Mineralogist* **42**, 619–630. https://doi.org/10.2113/gscanmin.42.2.619.

Tolstykh, N., Kozlov, A. & Telegin, Y. (2015). Platinum mineralization of the Svetly Bor and Nizhny Tagil intrusions, Ural Platinum Belt. *Ore Geology Reviews* **67**, 234–243. https://doi.org/10.1016/j.oregeorev.2014.12.005.

Tomlinson, E. L. & Holland, T. J. B. (2021). A thermodynamic model for the subsolidus evolution and melting of peridotite. *Journal of Petrology* **62**. https://doi.org/10.1093/petrology/egab012.

Tredoux, M., Lindsay, N. M., Davies, G. & McDonald, I. (1995). The fractionation of platinum-group elements in magmatic systems, with the suggestion of a novel causal mechanism. *South African Journal of Geology* **98**, 157–167.

Wang, A., Dhamelincourt, P. & Turrell, G. (1988). Raman microspectroscopic study of the cation distribution in amphiboles. *Applied Spectroscopy* **42**, 1441–1450. https://doi.org/10.1366/0003702884429490.

Xiong, Y. & Wood, S. A. (2000). Experime\uline{a}ntal quantification of hydrothermal solubility of platinum-group elements with special reference to porphyry copper environments. *Mineralogy and Petrology* **68**, 1–28. https://doi.org/10.1007/s007100050001.

Yan, H., Liu, Z., Di, J. & Ding, X. (2022). Crystal growth of osmium(IV) dioxide in chlorine-bearing hydrothermal fluids. *Minerals* **12**. https://doi.org/10.3390/min12091092.

Yudovskaya, M. A., Tessalina, S., Distler, V. V., Chaplygin, I. V., Chugaev, A. V. & Dikov, Y. P. (2008). Behavior of highly-siderophile elements during magma degassing: a case study at the Kudryavy volcano. *Chemical Geology* **248**, 318–341. https://doi.org/10.1016/j.chemgeo.2007.12.008.

Deltech Furnaces

Sustained operating temperatures to 1800° Celsius

www.deltechfurnaces.com

Gas Mixing System

An ISO 9001:2015 certified company

Custom Vertical Tube

ASME NQA-1 2008 Nuclear Quality Assurance

Standard Vertical Tube

Control systems are certified by Intertek UL508A compliant

Bottom Loading Vertical Tube